Progress Towards Cavity Induced Transparency

by

Tracy Li

Submitted to the Department of Physics
in partial fulfillment of the requirements for the degree of

Bachelor of Science in Physics

at the

MASSACHUSETTS INSTITUTE OF TECHNOLOGY
[June 2010]
May 2010

Author .....
Department of Physics
May 21, 2010

Certified by .....
Vladan Vuletić
Lester Wolfe Associate Professor of Physics
Thesis Supervisor

Accepted by .....
David E. Pritchard
Cecil and Ida Green Professor of Physics, Senior Thesis Coordinator

Progress Towards Cavity Induced Transparency

by

Tracy Li

Submitted to the Department of Physics
on May 21, 2010, in partial fulfillment of the
requirements for the degree of
Bachelor of Science in Physics

Abstract

Inspired by electromagnetically induced transparency (EIT), cavity induced transparency (CIT) uses a cavity rather than a laser to couple a ground state with the excited state of a three-level system. In this thesis, I discuss the theory behind CIT and present the progress in our current experiment aimed at achieving CIT. In particular, I discuss the technical aspects of the experiment and give an overview of our experimental setup. I conclude with preliminary data on the waist-size of the sideprobe beam on the atomic ensemble trapped in an optical lattice. We measure the beam size at our ensemble to be around $5\mu m$. Although we have not yet measured the size of the atomic cloud, we expect this beam size to be smaller than the atomic cloud, and hence our beam is maximally interacting with the atoms.

Thesis Supervisor: Vladan Vuletić
Title: Lester Wolfe Associate Professor of Physics

Acknowledgments

This thesis would not have been possible without the efforts of many people. Special thanks to Vladan for giving me the opportunity to work in his lab and for so kindly taking the time to advise me during certain academic crises. To say that this experience single-handedly changed my perspective on physics would not be an exaggeration. I have learned so much in the past year, and it was mostly due to the wonderful people I worked with. Marko, Monica, Ian, and Andrew have all been willing to sacrifice their own time to explain away confusions. Haruka, Renate, Jon, and Wenlan are the people I worked most closely with and have been a constant source of support and inspiration. I would like to especially thank Haruka for being the best mentor one could hope for. Her infinite patience has truly helped me grow so much as a physicist past year.

Additionally, I would like to thank my mom for all the sacrifices she has made to make all these opportunities available to me. My friends J and E have always been there for me when I needed them. I truly would not have enjoyed my four years here nearly as much without you guys.

Contents

List of Figures

List of Tables

Chapter 1

Introduction

Electromagnetically induced transparency (EIT) is a phenomenon in which the effect of a medium on a electromagnetic field propagating through is eliminated [13]. It is a dramatic demonstration of quantum interference between radiative transitions in an atom. EIT schemes require a 3-level system. One such scheme, known as a Λ scheme is shown in figure 1-1. This configuration consists of two ground states $|1\rangle$ and $|2\rangle$ each coupled to an excited state $|3\rangle$ by seperate lasers with coupling strengths Ω_1 and Ω_2, respectively. Consequently, the probability amplitudes of $|1\rangle$ and $|2\rangle$ both contribute to the probability amplitude of $|3\rangle$. When the detunings of both lasers are equal, the probability amplitude of $|3\rangle$ is zero due to quantum interference. This means that the absorption profile for one field is modified by the presence of a second field so that there is a narrow dip in the center of the absorption peak, where there would normally be maximum absorption!

Our experiment is in the spirit of EIT. Instead of using a laser beam to couple the $|2\rangle$ and $|3\rangle$ states, we will use a cavity. Rather than using electromagnetic fields to induce transparency, we use the cavity to induce transparency. Fittingly, this is called cavity induced transparency (CIT). CIT allows us to explore the interactions of an ensemble of atoms strongly coupled to a cavity. In our experiment, we use cesium atoms and probe on different hyperfine states of the $6^2S_{1/2} \rightarrow 6^2P_{3/2}$ line.

In Chapter 2, we discuss the semiclassical and quantum analysis of the two-level atom. We derive results that will be used in later sections. In Chapter 3, we discuss

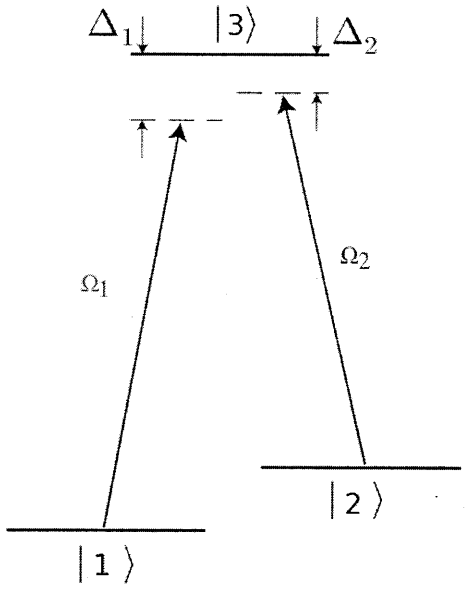

Figure 1-1: 3-level Lambda system

laser cooling and trapping techniques relevant to our experiment. Chapter 4 first presents the theory behind CIT and then discusses the experimental setup and technical aspects of the experiment. We also present some promising preliminary data. Chapter 5 ends with the conclusion.

Chapter 2

Atom-Field Interactions: The Two-Level Atom and Cavity QED

In this chapter, we examine the effects of a time-dependent external electromagnetic field on a two-level atom. Although an atom has an infinite number of bound states, the two-level atom problem is still of practical interest. When the external field is weak and near-resonance with a single atomic transition, we can neglect transitions to other levels and approximate an atom as a two-level system. There are two formalisms commonly used to describe the interaction between a two-level atom and an external field. We begin with the semiclassical theory, which treats the atom as a quantum two-level system and treats the field classically. A quantum mechanical treatment of the atom allows us to examine quantum coherences between the two levels and gives results we later use when examining dipole traps. However, the semiclassical treatment does not suffice. There are effects, such as the collapse and revival of atomic populations in the two states, that require a quantized field. Furthermore, more immediately related to our experiment, atom-photon interaction in a cavity is modeled by the interaction between an atom and a single mode of the quantized field. Hence, we also discuss a fully quantum theory, where both the atom and field are treated quantum mechanically.

2.1 The Two-Level Atom

Let the atom have ground state $|1\rangle$ and excited state $|2\rangle$ with energy difference $\hbar\omega_0$. To model the illumination of the atom by a laser, we assume a monochromatic classical field with frequency ω:

$$\mathbf{E}(t) = E_0 \cos(\omega t)\hat{\epsilon} = \mathcal{E}e^{i\omega t} + \mathcal{E}^* e^{-i\omega t} \tag{2.1}$$

where we have decomposed the electric field into its rotating components. Additionally, $\mathcal{E}$ is taken to be a vector. Note that we have made the dipole approximation: we have neglected the spatial dependence of the electric field by assuming that the electric field spatially varies on a much longer length scale than the size of the atom. This is appropriate in the case of optical transitions since atom size is on the order of angstroms while optical wavelengths are on the order of hundreds of nanometers [1].

The electric field induces and interacts with the atomic dipole, represented by operator $\hat{d} = e\hat{r}$. This operator can be conveniently expressed as

$$\hat{d} = \sum_{n,n'} |n'\rangle\langle n'|\hat{d}|n\rangle\langle n| = \sum_{n,n'} |n'\rangle\langle n|\langle n'|\hat{d}|n\rangle \tag{2.2}$$

Summing only the two relevant levels and substituting $\mu_{nn'} = \langle n'|\hat{d}|n\rangle$, we arrive at

$$\hat{d} = \mu_{12}|1\rangle\langle 2| + \mu_{21}|2\rangle\langle 1| \tag{2.3}$$

The Hamiltonian of the atom-field interaction, $\hat{H}_{AF}$, is given by the usual electric dipole Hamiltonian, $\hat{H}_{AF} = -\hat{d}\cdot\mathbf{E}$. Summing the atomic Hamiltonian $\hat{H}_A$ and atom-field interaction Hamiltonian $\hat{H}_{AF}$ gives the total Hamiltonian:

$$\hat{H} = \hat{H}_A + \hat{H}_{AF} = \hbar\omega_0|2\rangle\langle 2| - (\mu_{12}|1\rangle\langle 2| + \mu_{21}|2\rangle\langle 1|)\cdot(\boldsymbol{\mathcal{E}}e^{i\omega t} + \boldsymbol{\mathcal{E}}^* e^{-i\omega t}) \tag{2.4}$$

Using the Schroedinger equation $i\hbar\frac{d}{dt}|\psi\rangle = \hat{H}|\psi\rangle$ on the atomic state $|\psi\rangle = c_1(t)|1\rangle +$

$c_2(t)|2\rangle$ gives

$$\begin{aligned} \dot{c_2}(t) &= -i\omega_0 c_2(t) + \frac{i}{\hbar}(\mathcal{E}e^{-i\omega t} + \mathcal{E}^* e^{-i\omega t})\mu^* c_1(t) \\ \dot{c_1}(t) &= \frac{i}{\hbar}(\mathcal{E}e^{-i\omega t} + \mathcal{E}^* e^{-i\omega t})c_2(t) \end{aligned} \tag{2.5}$$

where we have defined $\mu = \mu_{12}$ (and hence, $\mu^* = \mu_{21}$.) We can simplify the above equations by transforming into a frame rotating with the electric field. This is equivalent to substituting $c_2(t) = \tilde{c_2}(t)e^{-i\omega t}$. The equations of motion become

$$\begin{aligned} \dot{\tilde{c}}_2(t) &= i\hbar\delta\tilde{c}_2(t) + \frac{i}{\hbar}(\mathcal{E} + \mathcal{E}^* e^{2i\omega t})\mu c_1(t) \\ \dot{\tilde{c}}_1(t) &= \frac{i}{\hbar}(\mathcal{E}^* + \mathcal{E}e^{-2i\omega t})\mu^* \tilde{c}_2(t) \end{aligned} \tag{2.6}$$

After this transformation, we find terms multiplied by $e^{\pm 2i\omega t}$. Since we are interested in dynamics that occur on timescales longer than the optical frequency ω, these terms can be neglected as the oscillations will average to zero. This is called the rotating wave approximation (RWA) and is valid when the field is weak and $\delta \equiv \omega - \omega_0 \ll \omega, \omega_0$. The equations of motion then become:

$$\begin{aligned} \dot{\tilde{c}}_2(t) &= i\delta\tilde{c_2}(t) + i\Omega c_1(t) \\ \dot{c}_1(t) &= i\Omega\tilde{c}_2(t) \end{aligned} \tag{2.7}$$

where $\Omega \equiv \frac{\varepsilon\mu}{\hbar}$. We can uncouple and solve the differential equations in 2.7 by differentiating the expression for $\dot{c_1}(t)$ and then substituting the expression for $\dot{c_2}(t)$. Using intial conditions $c_1(0) = 1$ and $c_2(0) = 0$, we arrive at

$$\begin{aligned} c_2(t) &= -i\frac{\Omega}{\Omega'}\sin\frac{\Omega' t}{2} \\ c_1(t) &= \cos\frac{\Omega' t}{2} - i\frac{\delta}{\Omega'}\sin\frac{\Omega' t}{2} \end{aligned} \tag{2.8}$$

where $\Omega' \equiv \sqrt{\Omega^2 + \delta^2}$.

Squaring the amplitudes gives us the probability of an atom occupying the excited

and ground states:

$$P_e = \frac{\Omega^2}{\Omega'^2}\sin^2\frac{\Omega' t}{2}$$
$$P_g = \cos^2\frac{\Omega' t}{2} + \frac{\delta^2}{\Omega'^2}\sin^2\frac{\Omega' t}{2} \tag{2.9}$$

These expressions tell us that the electric field causes the atom to oscillate between states $|1\rangle$ and $|2\rangle$, a phenomenon termed "Rabi flopping."

Furthermore, after moving to the rotating frame and making the RWA, we can write the Hamiltonian in matrix-form:

$$\hat{H} = \frac{\hbar}{2}\begin{bmatrix} -2\delta & \Omega \\ \Omega & 0 \end{bmatrix} \tag{2.10}$$

We diagonalize 2.10 to find the eigenengergies and eigenstates of the coupled Hamiltonian. The new eigenstates are mixtures of the bare atomic states. The eigenenergies are

$$E_{1,2} = \frac{\hbar}{2}(-\delta \pm \Omega') \tag{2.11}$$

Hence, another effect of the electric field is to shift the energies of $|1\rangle$ and $|2\rangle$ closer together for positive detuning δ or further apart for negative detuning δ.

2.2 Two-level Atom in a Cavity

Although many of the phenomena observed in atomic physics can be explained by the semi-classical theory, there are also many effects that require a quantum treatment of the field. Most basically, a quantized field introduces the concept of photons or quanta of energy. The eigenstates of the field Hamiltonian correspond to the number of photons present while the eigenvalues correspond to the total energy of the photons present. Furthermore, we know that an excited atom can transition to a lower energy state by emitting a photon even in the absence of an electromagnetic field. This "spontaneous emission" occurs due to atomic interactions with vacuum modes of the field—a result that can only be explained by a quantized field. In this section, we begin

by quantizing the electromagnetic field, closely following the procedure in reference [2]. Next, we derive the Jaynes-Cummings Hamiltonian, which models single-photon processes due to atom-photon interactions in a high-finesse cavity.

2.2.1 Quantization of electromagnetic fields

Consider an electric field inside a large cavity of length L and volume V. The normal modes of this cavity are running waves with wavevectors $k_{j\alpha} = \frac{2\pi j_\alpha}{L}$, where $j = (1, 2, 3...)$ is the mode number and $\alpha = (x, y, z)$ refers to the polarization direction. For convenience, from now on let the index j include information about both the mode number and the polarization direction. An electric field polarized in the x-direction propagating in the z-direction can be expressed in terms of these eigenmodes as

$$E_x(z,t) = \sum_j \sqrt{\frac{\omega_j^2}{\epsilon_0 V}} q_j e^{ik_j z} \tag{2.12}$$

where q_j is the mode amplitude and $\omega_j = \frac{cj}{L}$ is the cavity resonance frequency. Letting $A_j = \sqrt{\frac{\omega_j^2}{\epsilon_0 V}}$, the corresponding magnetic field given by Maxwell's equations is

$$B_y(z,t) = \frac{1}{c^2} \sum_j \frac{\dot{q}_j}{k_j} A_j e^{ik_j z} \tag{2.13}$$

We arrive at the classical Hamiltonian for the field inside the cavity by integrating the energy density due to the electric and magnetic fields over the volume of the cavity:

$$\begin{aligned} \hat{H}_{cav} &= \frac{1}{2} \int dV (\epsilon_0 E^2 + \frac{1}{\mu_0} B^2) \\ &= \sum_j \frac{\omega_j^2 q_j^2}{2} + \frac{\dot{q}_j^2}{2} \end{aligned} \tag{2.14}$$

Equation 2.14 is equivalent to the Hamiltonian of a set of harmonic oscillators with position q_j, frequency ω_j, and unit mass. Hence, the problem of field quantization is identical to the problem of harmonic oscillator quantization, where we identify q_j with the position operator $\hat{q}_j$ and $\dot{q}_j$ with the momentum operator $\hat{p}_j$. Consequently,

we obtain:

$$\hat{H}_{cav} = \hbar \sum_j \omega_j (\hat{a}_j^\dagger \hat{a}_j + \frac{1}{2}) \tag{2.15}$$

where $\hat{a}_j$ and $\hat{a}_j^\dagger$ are the standard creation and annihilation operators for mode j. In this context, $\hat{a}$ annihilates a photon and $\hat{a}^\dagger$ creates a photon in the cavity.

Writing $\hat{q}$ in terms of the annihilation and creation operators gives the electric field with polarization vector ϵ_α in terms of $\hat{a}_j$ and $\hat{a}_j^\dagger$ as

$$\hat{E}_\alpha = \epsilon_\alpha \sqrt{\frac{\hbar\omega_j}{\epsilon_0 V}} (\hat{a}_j + \hat{a}_j^\dagger) e^{i\mathbf{k}_j \cdot \mathbf{r}} \tag{2.16}$$

$$= \hat{\varepsilon_\alpha} + \hat{\varepsilon_\alpha^\dagger} \tag{2.17}$$

where $\hat{\varepsilon} = \epsilon_\alpha \sum_j \sqrt{\frac{\hbar\omega_j}{2\epsilon_0 V}} \hat{a}_j e^{i\mathbf{k}_j \cdot \mathbf{r}}$.

2.2.2 The Jaynes-Cummings Hamiltonian

Interactions between a single atom and a single mode field can be experimentally realized by using a high-finesse cavity to isolate a single mode field (the "cavity mode" field) and confine a single atom. The total Hamiltonian for this system is the sum of the atomic, field, and atom-field interaction Hamiltonians:

$$\hat{H} = \hat{H}_A + \hat{H}_F + \hat{H}_{AF} = \hbar\omega_0 |2\rangle\langle 2| + \hbar\omega_c (\hat{a}^\dagger \hat{a} + \frac{1}{2}) + \hat{H}_{AF} \tag{2.18}$$

where the cavity mode has frequency ω_c with field operators $\hat{a}$ and $\hat{a}^\dagger$. As in the semi-classical case, the atom-field interaction Hamiltonian is a dipole Hamiltonian $\hat{H}_{AF} = -\hat{d} \cdot \hat{E}$, where $\hat{E}$ takes the form of 2.16. We find four terms after taking the dot product:

$\hat{a}^\dagger |1\rangle\langle 2|$: Atom decays and emits a photon

$\hat{a} |2\rangle\langle 1|$: Atom is excited and absorbs a photon

$\hat{a}^\dagger |2\rangle\langle 1|$: Atom is excited and emits a photon

$\hat{a} |1\rangle\langle 2|$: Atom decays and absorbs a photon

The first two processes do conserve energy while the last two processes do not conserve energy and can be neglected. This situation is equivalent to the RWA approximation in the semi-classical theory and is valid under the same conditions.

After making the RWA approximation, the atom-field interaction Hamiltonian is

$$\hat{H}_{AF} = -\hbar g(\hat{a}|2\rangle\langle 1| + \hat{a}^\dagger|1\rangle\langle 2|) \tag{2.19}$$

where $g = \frac{\mu}{\hbar}\sqrt{\frac{\hbar\omega_c}{2\epsilon_0 V}}e^{i\mathbf{k}\cdot\mathbf{r}}$ is the cavity QED coupling constant (which is analogous to Ω in the semi-classical picture.) This gives the total Jaynes-Cummings Hamiltonian as

$$\hat{H} = \hbar\omega_0|2\rangle\langle 2| + \hbar\omega_c(\hat{a}^\dagger\hat{a} + \frac{1}{2}) - \hbar g(\hat{a}|2\rangle\langle 1| + \hat{a}^\dagger|1\rangle\langle 2|) \tag{2.20}$$

We can investigate the dynamics of the Jaynes-Cummings model with the same procedure used in the semi-classical model. Written in the basis of the the uncoupled Hamiltonian, the state vector is $|\psi\rangle = \sum_n c_{1,n}(t)|1,n\rangle + c_{2,n}|2,n\rangle$. From equation (2.19), we see that the only possible transitions are between states $|1,n+1\rangle$ and $|2,n\rangle$. The transition from $|1,n+1\rangle$ to $|2,n\rangle$ corresponds to the atom in the ground state $|1\rangle$ with $n+1$ photons in the cavity absorbing a photon, which results in an excited atom in the $|2\rangle$ state with n photons in the cavity. Applying Schroedinger's equation and projecting with $\langle 2,n|$ and $\langle 1,n+1|$, we obtain the following amplitudes:

$$\begin{aligned}\dot{c}_{2,n} &= -i(\omega_0 + n\omega_c)c_{2,n} + ig\sqrt{n+1}c_{1,n+1} \\ \dot{c}_{1,n+1} &= -i(n+1)\omega_c c_{1,n+1} + ig\sqrt{n+1}c_{2,n}\end{aligned} \tag{2.21}$$

This looks a lot like our amplitude equations in (2.7) from the semi-classical model. In fact, the two are formally equivalent with a Rabi frequency $\Omega_n = 2g\sqrt{n+1}$ and detuning $\omega_c - \omega_0 = \delta$. Like the semi-classical model, the eigenstates of the Jaynes-Cummings Hamiltonian are mixtures of the uncoupled states, $|1,n+1\rangle$ and $|2,n\rangle$, and the off-resonant Rabi frequency is $\Omega_n' = \sqrt{\Omega_n^2 + \delta^2} = \sqrt{4g^2(n+1) + \delta^2}$.

Chapter 3

Laser Cooling and Trapping

Laser cooling and trapping are integral tools in the field of atomic physics. Cooling and trapping atoms allows us to explore ultra-low energy regions and gives us unprecedented control over atomic motion. In this chapter, we begin with the most basic cooling scheme, Doppler cooling, which damps the velocity of the atoms. We next discuss the magneto-optical trap (MOT), which uses magnetic and optical fields to provide both cooling and a confining potential. Polarization gradient cooling (PGC) cools atoms below the Doppler cooling limit by using the polarization gradient resulting from counterpropagating beams and the multilevel structure of atoms. Finally, we discuss the optical dipole trap, optical lattices, and derive the axial and radial trap frequencies. This order roughly mimics the order in which we would experimentally proceed when loading a dipole trap.

3.1 Doppler Cooling

Qualitatively, Doppler cooling works by using two counterpropagating beams to illuminate an atom. The frequency of both beams is detuned slightly below a specific atomic transition frequency. If an atom moves with velocity $\mathbf{v}$ toward a beam with wavevector $\mathbf{k}$ and assuming colinear motion, the atom will see the frequency of the beam increase by kv due to the Doppler effect. Similarly, the atom will see the frequency of the beam it moves away from decrease by kv. Since the detuning δ is

negative, the atom will preferentially absorb photons from the beam it moves towards. The momentum transfer due to this preferential absorption decreases the kinetic energy and hence temperature of the atom. There is no net momentum effect from emission of photons since the atom emits in all directions. Doppler cooling is dependent on this lack of net momentum effect from emissions so that the net momentum effect from absorptions will dominate. Consequently, it is important that our beams have low intensity because it allows us to ignore stimulated emission. Stimulated emission results in a preferred direction of emission, which results in a net momentum that cancels out the effect from preferential absorption.

Quantitatively, the force on a moving atom due to a traveling wave is

$$\mathbf{F} = \frac{\hbar\gamma\mathbf{k}}{2}\frac{s_0}{1+s_0+(\frac{2(\delta-\mathbf{k}\cdot\mathbf{v})}{\gamma})^2} \tag{3.1}$$

where γ corresponds to the decay rate of the excited state and s_0 is the saturation parameter. In the case of low light intensity, the total force on the atom is simply the sum of the force from each beam:

$$\mathbf{F}_{om} = \frac{s_0\hbar\gamma\mathbf{k}}{2}\left(\frac{1}{1+s_0+(\frac{2(\delta-\mathbf{k}\cdot\mathbf{v})}{\gamma})^2} - \frac{1}{1+s_0+(\frac{2(\delta+\mathbf{k}\cdot\mathbf{v})}{\gamma})^2}\right) \tag{3.2}$$

$$\approx \frac{8\hbar\delta s_0 k^2}{\gamma(1+s_0+(\frac{2\delta}{\gamma})^2)^2}\mathbf{v} \equiv -\beta\mathbf{v} \tag{3.3}$$

where we have expanded in $\frac{kv}{\delta}$ to first order in (3.3). From equation (3.3), we see why this technique is aptly referred to as an optical molasses this slowing force results in viscous damping. The force is plotted in figure 3-1. For small velocities, the force mimics the usual linearly dependent damping force. After a critical velocity, the force decreases rapidly. Note that Doppler cooling only damps the velocity and does not actually trap the atoms.

So far our treatment seems to imply that the damping force can completely decelerate an atom and bring its temperature all the way down to absolute zero, violating thermodynamics. What we have neglected to do is include heating effects due to the

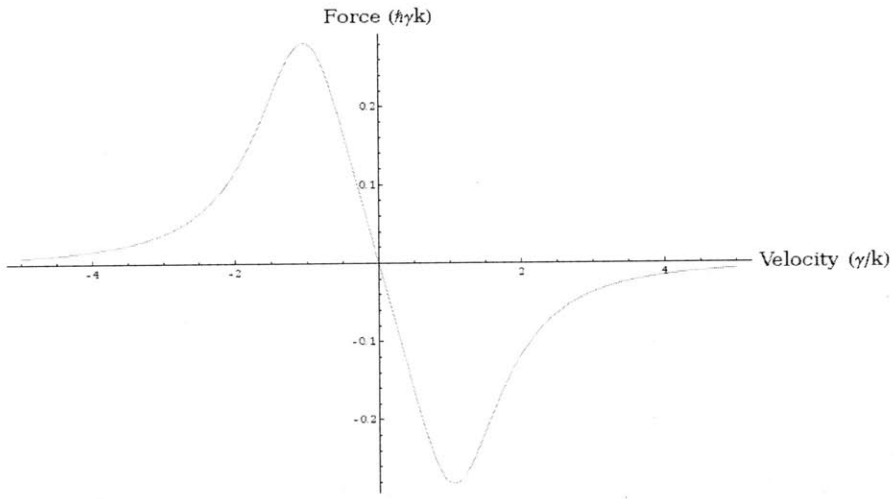

Figure 3-1: Optical molasses cooling force. Plotted with $s_0 = 2, \delta = -\gamma$. The force rapidly diminishes for atoms with velocities greater than the capture velocity.

momentum transfers from the absorption and emission of photons. Each momentum transfer on average imparts recoil energy $E_r = \frac{\hbar^2 k^2}{2m}$ to the atom, which results in heating. Hence, there is a lower temperature limit to Doppler cooling, which is typically below 1mK [3].

3.2 Magneto-Optical Trap

The magneto-optical trap (MOT) uses optical fields and a magnetic field gradient to simultaneously cool and trap atoms. In a MOT, anti-Helmholtz coils are used to create a constant magnetic field gradient that vanishes in the center of the trap. This is where the atoms will accumulate. By the Zeeman effect, an atomic transition will split into its magnetic sublevels in the presence of a magnetic field. Each sublevel is shifted by energy $\Delta E_Z = \mu_b m_j g_j B_0$, where μ_b is the Bohr magneton, m_j is the magnetic quantum number that projects the total angular momentum onto the quantization axis, g_j is the Lande g-factor, and B_0 is the magnitude of the magnetic field. The presence of a magnetic field gradient results in position-dependent energy shifts. Position-dependent energy shifts means that at any point in the MOT, certain transitions between magnetic sublevels (in accordance with selection rules) will be

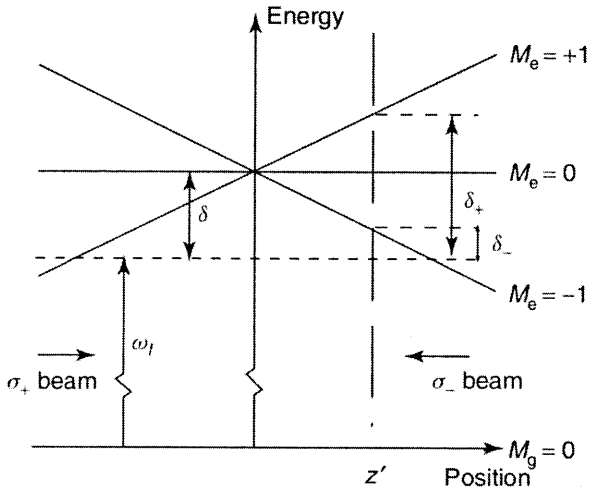

Figure 3-2: Diagram for 1D MOT. At position z, atoms preferentially absorb σ^- light, resulting in a net force pushing the atom toward the trap center. ω_l is the frequency of the laser, δ is the detuning from the $m_g = 0 \rightarrow m_e = 0$ transition, δ_+ is the detuning from the $m_g = 0 \rightarrow m_e = +1$ transition, and δ_- is the detuning from the $m_g = 0 \rightarrow m_e = -1$ transition. Figure from [3]

less detuned than other transitions. We can selectively address these transitions by using counterpropagating beams with σ^+ and σ^- polarizations. σ^+ polarized light induces $\Delta m_j = 1$ transitions while σ^- polarized light induces $\Delta m_j = -1$ transitions from the ground state to the excited state. The arrangement of the 1D MOT with the simplest case of a transition from ground state $J_g = 0$ to an excited state $J_e = 1$ is shown in figure 3-2. In reference to the figure, consider an atom at position z, on the right side of the trap center. Since the beam is less detuned from the $\Delta m_j = -1$ transition, the atom will preferentially absorb photons from the σ^- polarized beam. If we choose the σ^- beam to be incident from the right (and incidentally, the σ^+ beam is incident from the left), the atom will be pushed toward the center in a manner analogous to the Doppler cooling situation.

Quantitatively, we can easily modify the force equation for the optical molasses in 3.2 to apply to our 1D MOT scheme. We need only to take into account an additional frequency shift in the detuning due to the Zeeman energy shifts. Hence, we replace the $\delta \pm \mathbf{k} \cdot \mathbf{v}$ by $\delta \pm \mathbf{k} \cdot \mathbf{v} \mp \frac{\mu B_0 z}{\hbar}$ in the denominators of 3.2, where we have substituted $\mu B_0 z$ for ΔE_Z. Taylor expanding to first order in $\frac{k}{\delta}(\mathbf{k} \cdot \mathbf{v} + \frac{\mu B_0 z}{\hbar})$ gives the MOT force

as

$$\begin{aligned}\mathbf{F}_{MOT} &= \frac{8\hbar\delta s_0 k^2}{\gamma(1+s_0+(\frac{2\delta}{\gamma})^2)^2}\mathbf{v} + \frac{8\delta^2 s_0 k\mu B_0}{\gamma(1+s_0+(\frac{2\delta}{\gamma})^2)^2}\mathbf{z} \\ &= -\beta\mathbf{v} - \kappa\mathbf{z} \end{aligned} \tag{3.4}$$

Equation 3.4 is equivalent to the force equation of a damped harmonic oscillator and shows that the MOT provides both a viscous damping force and a restoring force. Although we have only examined a 1D MOT, this discussion can be generalized for a 3D MOT by simply placing counterpropagating beams on all three axes.

3.3 Polarization Gradient Cooling

The temperature limit of Doppler cooling was long believed to be a fundamental limit in cooling schemes. However, in the late 1980's, experiments with alkali metals resulted in limits more than ten times lower! Sub-Doppler cooling was first explained by Cohen-Tannoudji and collaborators in a scheme known as polarization gradient cooling (PGC) or Sisyphus cooling [5]. This technique considers the resultant field inhomogeneity of counterpropagating beams and the multilevel structure of atoms.

Consider the sum of two linearly polarized, orthogonal, counterpropagating beams with the same frequency ω and magnitude E_0

$$\begin{aligned}\mathbf{E} &= E_0\cos(\omega t + kz)\hat{x} + E_0\cos(\omega t - kz)\hat{y} \\ &= E_0\cos(\omega t)\cos(kz)(\hat{x}+\hat{y}) + E_0\sin(\omega t)\sin(kz)(\hat{x}-\hat{y}) \end{aligned} \tag{3.5}$$

At $z = 0$, $\mathbf{E} = E_0\cos(\omega t)(\hat{x}+\hat{y})$. The field is linearly polarized along an axis tilted $\frac{\pi}{4}$ from the x-axis. At $z = \frac{\lambda}{8}$, $\mathbf{E} = E_0\sin(\omega t + \frac{\pi}{4})\hat{x} - E_0\cos(\omega t + \frac{\pi}{4})\hat{y}$. The field is circularly polarized in the negative sense about the z-axis (polarization σ^-.) Similarly, at $z = \frac{\lambda}{4}$, the field is once again linearly polarized but along an axis titled $-\frac{\pi}{4}$ from the x-axis. At $z = \frac{3\lambda}{8}$, the field is circularly polarized in the positive sense about the z-axis (polarization σ^+.) We see that there is a strong polarization gradient. This is

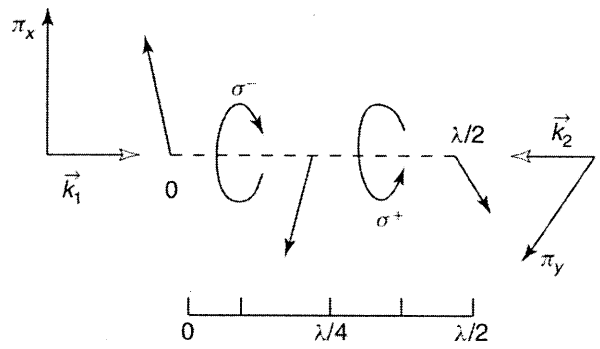

Figure 3-3: Spatial dependence of the polarization of linearly polarized counterpropagating beams.

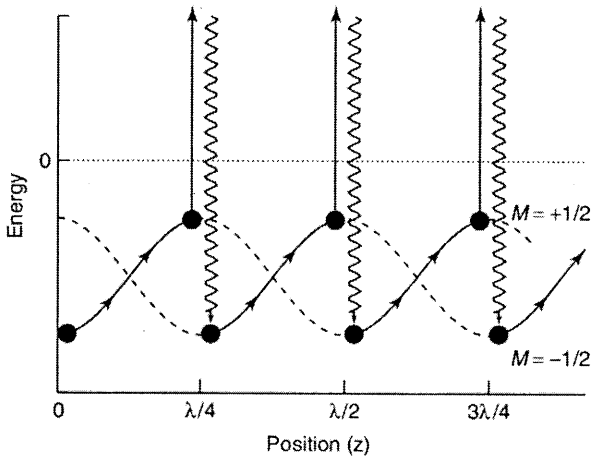

Figure 3-4: Spatial dependence of energy shifts of ground state magnetic sublevels, $m_g = 1/2$ and $m_g = -1/2$. Solid lines show energy path of atoms being cooled.

illustrated in figure 3-3

Now consider PGC running on a simple $J_g = 1/2 \rightarrow J_e = 3/2$ transition. The two ground state magnetic sublevels $m_g = \pm 1/2$ undergo different light shifts due to the σ^+ and σ^- field polarizations. Hence, they are not energetically degenerate even in the absence of a magnetic field. Where $m_g = 1/2$ has energy maxima, $m_g = -1/2$ has energy minima, and vice versa. This is depicted in figure 3-4.

Say the atoms start out in a region of space where the field has σ^+ polarization. Due to dipole selection rules, the ground state magnetic sublevel $m_g = 1/2$ can only couple to the excited state magnetic sublevel $m_e = 3/2$ and decay back to

$m_g = 1/2$. Similarly, the ground state magnetic sublevel $m_g = -1/2$ can only couple to $m_e = 1/2$ and can decay back to either $m_g = 1/2$ or $m_g = -1/2$. The Clebsch-Gordan coefficients tell us that it is twice more likely for $m_e = 1/2$ to decay into $m_g = 1/2$ than $m_g = -1/2$. Hence, the net effect of the σ^+ polarized field is to pump atoms from $m_g = -1/2$ to $m_g = 1/2$. In σ^+ polarized, the $m_g = 1/2$ state has lower energy than the $m_g = -1/2$ state. Similarly, in σ^- light, the $m_g = -1/2$ state has lower energy and the light pumps atoms from the $m_g = 1/2$ state to the $m_g = -1/2$ state.[1] As an atom in the $m_g = 1/2$ state moves in the σ^+ region toward the σ^- region, it converts kinetic energy into potential energy. As it reach the top of the potential hill and is about to convert the gained potential energy back into kinetic energy, the σ_- light intervenes and pumps the atoms into the $m_g = -1/2$ state. The previously gained potential energy is lost with the emission of a photon. The process repeats until the atom no longer has enough energy to surmount the potential hill, or equivalently, move by $\lambda/4$.

Like in Doppler cooling, heating is introduced through the momentum kicks the emitted photon imparts to the atom. The cooling limit scales as $\frac{\hbar k^2}{2m}$. Figure 3-5.shows both the Doppler and PGC cooling force. Note the smaller capture velocity but larger damping of PGC.

3.4 Optical Dipole Trap

Since PGC cannot operate in the presence of a magnetic field, we must again confine the atoms once they have been further cooled. We use an optical dipole trap [16]. Optical dipole traps work through the interaction between the atomic dipole and the laser field. As previously discussed, an atom does not have a permanent electric dipole. Rather, an oscillating atomic dipole moment is induced by the oscillating electric field of the laser. This dipole moment then interacts with the electric field. Along with other interesting effects, this results in a shift in the energy levels of the

[1] Linearly polarized light has no net pumping effect on the atoms; the Clebsch-Gordan coefficients tell us that the atoms will decay back to the state they came from.

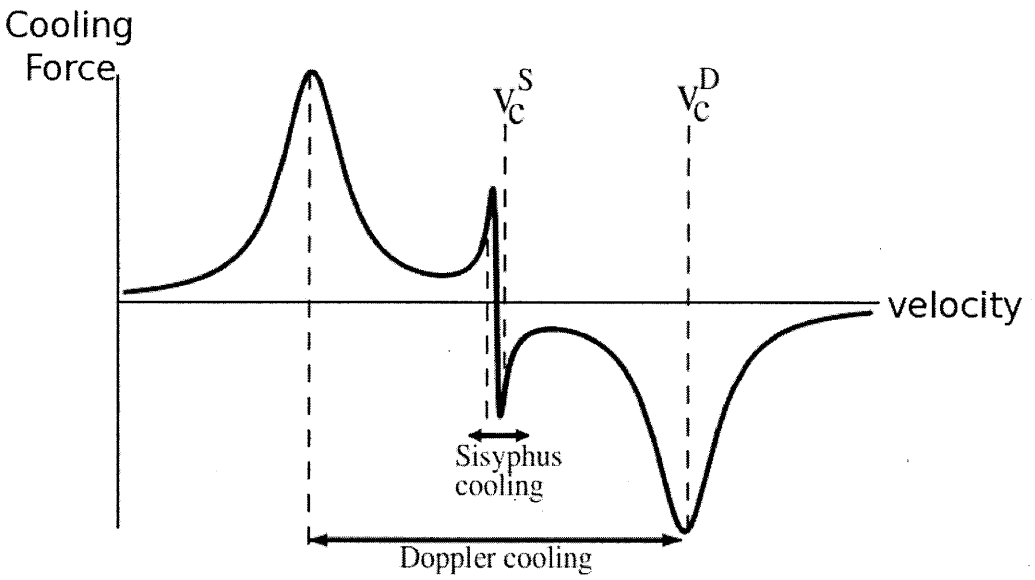

Figure 3-5: Plot of Doppler cooling and PGC force. Figure from [4].

atom (i.e. the Stark shift.) If the laser field is spatially inhomogeneous, the energy shifts will be correspondingly inhomogeneous. This creates a potential, and the force from this potential is the optical dipole force [17].

We have conveniently already derived the Stark shift in 2.11. In the limit where $\Omega \ll |\delta|$, the Stark shift ΔE_S is

$$\Delta E_S = \frac{\hbar \Omega^2}{4\delta} \tag{3.6}$$

to first order. Since the laser field is spatially inhomogeneous, Ω is no longer a constant and is instead spatially dependent $\Omega(r)$, where r refers to the spatial coordinate over which the field varies. The on-resonance saturation parameter s_0 relates $\Omega(r)$ with the intensity of the field, $I(r)$: $s_0 \equiv \frac{2|\Omega(r)|^2}{\gamma^2} = I(r)/I_s$, where I_s is the saturation intensity [3]. For a focused Gaussian beam, the intensity is given by $I(r,z) = \frac{2P}{\pi w(z)^2} e^{\frac{-2r^2}{w(z)^2}}$, where r is the radial coordinate, P is the power of the beam, and $w(z)$ gives the axial dependence of the beam radius as

$$w(z) = w_0 \sqrt{1 + (\frac{z}{z_R})^2} \tag{3.7}$$

where w_0 is the minimum radius of the beam (the beam waist) and $z_R = \frac{\pi w_0^2}{\lambda}$ (the Rayleigh range.) In our experiment, a standing wave is formed in our cavity due to the constructive interference of the laser beam. This configuration is called an optical lattive. In optical lattices, there is also an axial variation in the beam intensity. To account for this, we simply multiply our previous intensity equation by $\cos^2(kz)$. Plugging our expression for the beam intensity into 3.6, the spatially dependent potential is

$$U(r,z) = \frac{U_0}{1+(\frac{z}{z_R})^2}\cos^2(kz)e^{\frac{-2r^2}{w(z)^2}} \tag{3.8}$$

where

$$U_0 = \frac{\hbar\gamma^2 P}{4\pi w_0^2 \delta I_s} \tag{3.9}$$

is the trap depth, defined at $U(r=0,z=0)$. The potential in 3.8 is Gaussian. We see that near its minimum, the potential looks similar to the potential of a harmonic oscillator. If the thermal energy of the atomic ensemble is much smaller than the trap depth, we can assume a small radial extension of the atoms.[2] Expanding the potential in $(\frac{r}{w_0})^2$ and $(\frac{z}{z_R})^2$ to first order gives

$$U(r,z) = -U_0\cos^2(kz)(1-\frac{2}{w_0^2}r^2 - \frac{1}{z_R^2}z^2) \tag{3.10}$$

This is indeed the potential of a harmonic oscillator. It follows that an atom of mass m oscillates with frequency $\omega_z = \sqrt{\frac{2U_0}{mz_R^2}}$ in the axial direction and frequency $\omega_r = \sqrt{\frac{4U_0}{mw_0^2}}$ in the radial direction.

There is a subtlety in our discussion of the dipole trap. We quite casually used the Stark shift of a two-level atom after making the RWA. But recall that the RWA is only valid when the the laser is near resonance with an atomic transition. This is not the case in the dipole trap—the laser field of the dipole trap is far detuned from atomic resonance since we do not want to excite the atom. Without the RWA approximation, we need to take into account the effect of all other atomic levels when calculating the energy shift by using perturbation theory.

[2]This is equivalent to saying we are within the Lamb-Dicke regime.

Chapter 4

Cavity induced transparency: the experiment

4.1 Theory behind cavity induced transparency

Consider ground states $|1\rangle$ and $|2\rangle$ and excited state $|3\rangle$ arranged in the Λ configuration shown in figure 4-1. In CIT, instead of the usual laser beam, the cavity is used to couple $|2\rangle$ to $|3\rangle$. From our discussion of the two-level atom, we can figure out the relevant Hamiltonian. In the rotating frame and after making the RWA, the uncoupled atomic Hamiltonian for a single atom and a single photon is

$$\hat{H}_a = \hbar\delta|1\rangle\langle 1| + \hbar\delta_c|2\rangle\langle 2| \tag{4.1}$$

where the energy of the excited state is zero, δ is the laser detuning from the $|1\rangle$ to $|3\rangle$ transition, and δ_c is the cavity detuning from the $|2\rangle$ to the $|3\rangle$ transition. The interaction Hamiltonian is

$$\hat{H}_{int} = \frac{\hbar\Omega}{2}|3\rangle\langle 1| + \hbar g|3\rangle\langle 2| + h.c \tag{4.2}$$

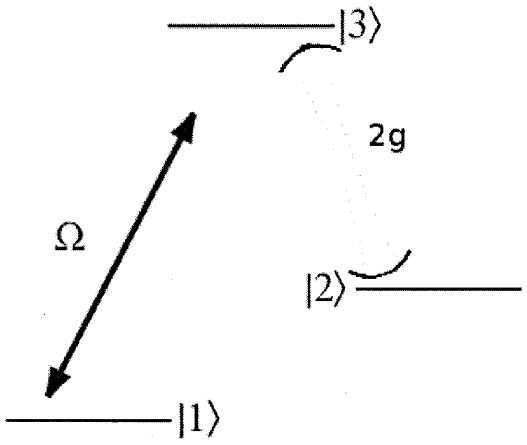

Figure 4-1: Λ configuration. The cavity couples $|2\rangle$ to $|3\rangle$ with coupling strength $2g$. A laser beam couples $|1\rangle$ to $|3\rangle$ with coupling strength Ω.

where Ω is the laser coupling strength and g is the cavity QED coupling constant. We can rewrite 4.2 as

$$\hat{H}_{int} = \frac{\hbar}{2}|3\rangle(\Omega\langle 1| + 2g\langle 2|) + h.c \tag{4.3}$$

This motivates transforming to a basis

$$\begin{aligned} |+\rangle &= \frac{1}{\sqrt{\Omega^2 + 4g^2}}(\Omega|1\rangle + 2g|2\rangle) \\ |-\rangle &= \frac{1}{\sqrt{\Omega^2 + 4g^2}}(\Omega|2\rangle - 2g|1\rangle) \end{aligned} \tag{4.4}$$

We can write $|1\rangle$ and $|2\rangle$ in the basis of $|+\rangle$ and $|-\rangle$. Substituting these expressions for $|1\rangle$ and $|2\rangle$ into (4.2) and (4.1) allows us to write the atomic and interaction Hamiltonians in the $|+\rangle$ and $|-\rangle$ basis:

$$\begin{aligned} \hat{H}_a &= \hbar\Delta_1|+\rangle\langle +| + \hbar\Delta_2|-\rangle\langle -| + \hbar\Omega'(|-\rangle\langle +| + |+\rangle\langle -|) \\ \hat{H}_{int} &= \frac{\hbar\sqrt{\Omega^2 + 4g^2}}{2}(|+\rangle\langle 3| + |3\rangle\langle +|) \end{aligned} \tag{4.5}$$

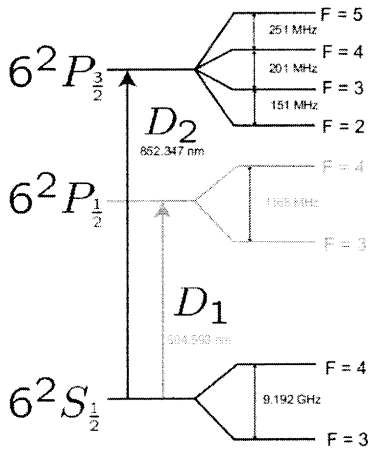

Figure 4-2: Energy level diagram for cesium. Figure from [10], splitting values from [11].

where $\Delta_1 = \frac{1}{\Omega^2+4g^2}(\Omega^2\delta + 4g^2\delta_c)$, $\Delta_2 = \frac{1}{\Omega^2+4g^2}(4g^2\delta + \Omega^2\delta_c)$, and $\Omega' = \frac{2g\Omega}{\Omega^2+4g^2}(\delta_c - \delta)$. We see from the interaction Hamiltonian that $|-\rangle$ is decoupled from $|3\rangle$. Furthermore, at Raman resonance, when $\delta_c = \delta$, $|-\rangle$ is also decoupled from $|2\rangle$. Therefore, if we were to scan the probe beam frequency while holding the cavity frequency constant, we would see a narrow dip in the absorption spectrum when the detuning of the cavity is the same as the detuning of the laser beam. This is same effect as EIT, but we have essentially used an empty cavity to modify the absorption spectra of the atoms![1]

4.2 Experimental implementation

A diagram of the lasers entering the vacuum chamber is in figure 4-3. The relevant level structures in cesium are shown in figure 4-2. In order to load the atoms into the optical lattice, both the lattice beam and three MOT beams are turned on. The atoms will accumulate in the overlapping area of the beams. The optical lattice beam is at 937nm. The MOT works on $F = 4$ ground state to the $F = 5$ excited state transition (henceforth called the $F = 5'$ state) on the cesium $|6^2S_{1/2}\rangle$ to $|6^2P_{3/2}\rangle$ line

[1]Perhaps you think we're cheating a little here. After all, the cavity isn't totally empty since the coupling in the cavity results from the photons emitted into the cavity mode. But the essential (and novel) point of the experiment is that the cavity starts out being empty and no beam is ever sent through the cavity to drive a transition.

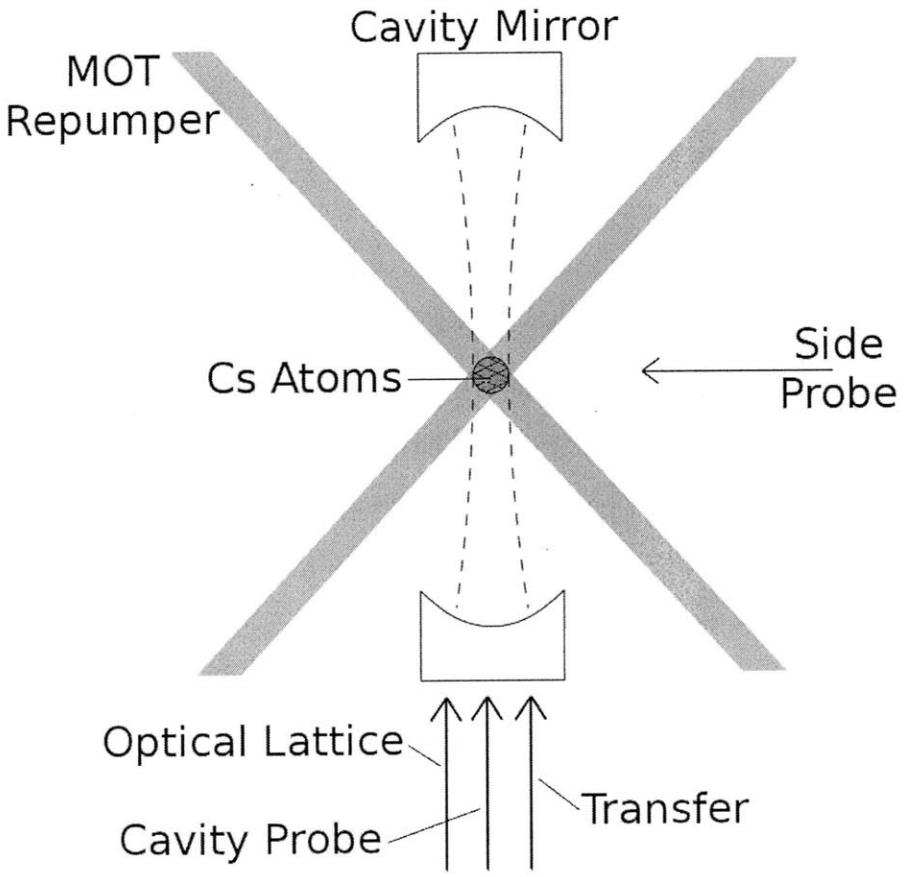

Figure 4-3: Diagram of cavity and lasers. MOT beams and repumper beams enter the vacuum on the same path. A third MOT beam enters perpendicular to the plane of the page.

at 852nm. It is also possible for an off-resonant excitation from $F = 4$ to $F = 4'$ to occur. Atoms in $F = 4'$ can decay into the $F = 3$. To prevent the loss of atoms in the cooling process, a repumper beam on the $F = 3$ to $F = 4'$ transition is used to repump atoms back to $F = 4$.

The MOT will cooling will be enough to trap some atoms in the optical lattice, but other atoms will require further cooling. This further cooling is achieved by using PGC. We use PGC on the $F = 3 \rightarrow F = 2'$ transition. A quick way of seeing why PGC is more effective than Doppler cooling is by comparing the force vs. velocity graphs of PGC and Doppler cooling in figure 3-5. PGC has a much greater damping coefficient as evidenced by the steeper slope, but also has a much smaller capture velocity. Hence, it is necessary to cool atoms prior to using PGC.

Once the dipole trap is loaded, we pump the atoms into the $F = 3$ state, and measure the transmission of the probe beam using a photodiode.

4.3 Preliminary Data: the size of the beam illuminating the atomic ensemble

To ensure our probe beam passes through the atomic ensemble in its entirety and maximal absorption occurs, we must make sure the probe beam waist is smaller than the width of the atomic ensemble and is centered on it. In order to measure the size of the probe beam when it passes through our atomic ensemble, we use the probe beam to excite atoms from the $F = 3$ ground state to the $F = 4$ excited state for a set amount of time. Atoms excited to the $F = 4'$ state will spontaneously decay into the $F = 4$ ground state. They will also spontaneously decay back into the $F = 3$ ground state, but we later account for this in our calculations. A beam is sent through the cavity to excite atoms from $F = 4$ to $F = 5'$. As we saw in the Jaynes-Cummings Hamiltonian, a Stark shift occurs between the dressed states $|F = 4, n\rangle$ and $|F = 5', n - 1\rangle$, where n is the number of photons in the cavity. This energy shift corresponds to a shift in the cavity resonance frequency. Therefore, by scanning

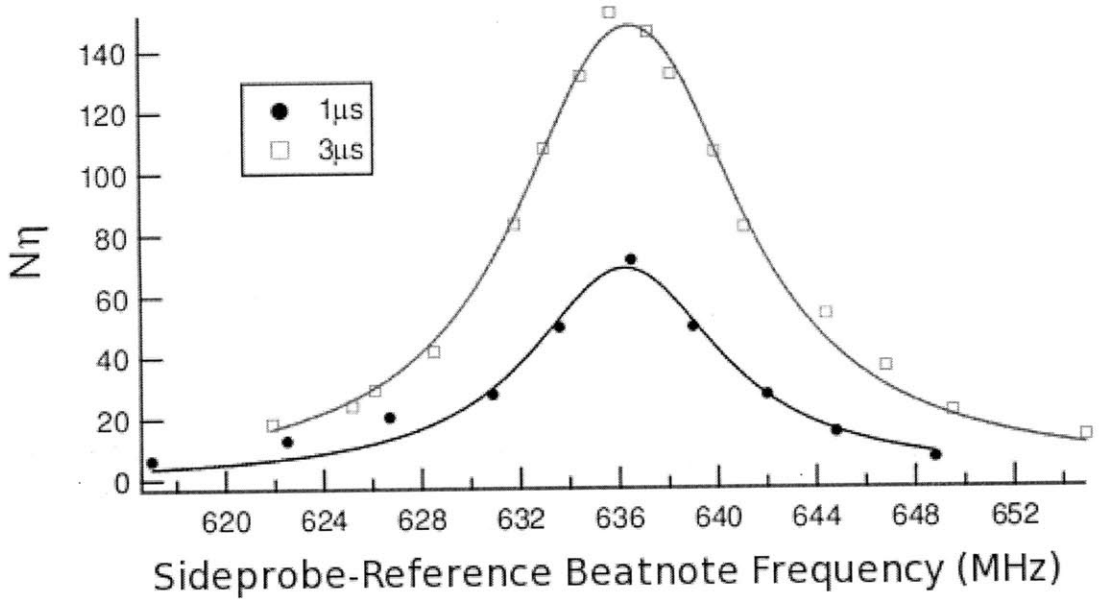

Figure 4-4: Fitted beam waist-size data. The sideprobe beam is turned on for $1\mu s$ and $3\mu s$.

the cavity beam and detecting the light that is transmitted through the cavity, we can obtain the cavity transmission peak and find the value of the energy shift. Next, we use the energy shift to obtain the number of atoms. For N atoms, the coupling between the ground and excited dressed states is $2g\sqrt{N}$, which gives the Stark shift as

$$\Delta E_s = \frac{g^2 N}{\delta} \tag{4.6}$$

We can write this shift in terms of the cooperativity parameter, $\eta = \frac{4g^2}{\kappa\gamma}$ giving

$$\Delta E_s = N\eta(\frac{\kappa\gamma}{4\delta}) \tag{4.7}$$

Since the energy shift is given by our data and we know parameters κ, γ, and δ, we can solve for $N\eta$. We then plot $N\eta$ as a function of the frequency difference between the reference laser and the probe laser. This is shown in figure 4-4.

The number of atoms that end up in the $F = 4$ state is not simply the number of atoms that were originally in the $F = 3$ state. Rather, we need to consider the

	$N\eta$	s_0	ω_0 (MHz)	beam size (μm)
$t = 1\mu s$	117.3	1.09	636.3	5.1
$t = 3\mu s$	170.1	0.67	636.5	4.6

Table 4.1: Summary of fit results and beam sizes from beam size data.

intensity of the laser and the decay rate from $F = 4'$ to $F = 4$. These factors are accounted for in a quantity called the scattering rate Γ:

$$\Gamma = \frac{\gamma}{2} \frac{s_0}{1 + s_0 + (\frac{2\delta}{\gamma})^2} \tag{4.8}$$

where s_0 is the ratio between the beam intensity and the saturation intensity. The number of atoms that end up in the $F = 4$ state is

$$N(\delta) = N_0(1 - e^{-\alpha\beta\Gamma t}) \tag{4.9}$$

where $\beta = 0.58$ is the branching ratio of the decay from the $F = 4'$ state into the $F = 4$ state, α is the oscillator strength between $F = 3$ to $F = 4'$, t is the time the probe beam illuminates the atoms, and N_0 is the number of atoms initially in the $F = 3$ state. We can fit our data to (4.9) with parameters N_0, ω_0, and s_0. Once we obtain s_0, we can obtain the intensity. Since we know the beam power, P, and $I = \frac{2P}{\pi w_0^2}$ because the beam is Gaussian, we can solve for $w_0 = \sqrt{\frac{2P}{I\pi}}$. The fit data and beam size data is summarized in table 4.1. Discrepancies in the data may be due to the laser linewidth or spatial saturation effects. The beam sizes may be an overestimation. They are only true if all the all the incident power illuminates the atomic ensemble, which would only be the case in a perfectly collimated beam with no spherical abberation at the lenses. Therefore, estimating that around 50% of the incident power is at the center of the beam may be more realistic. Hence, it is likely that our actual beam sizes are smaller by a factor of $\sqrt{(2)}$.

4.4 Laser and Cavity Locking Schemes

The success of our experiment depends crucially on the ability to stabilize our laser frequencies and cavity widths. Our relevant atomic transitions have a natural linewidth of $\approx$ 5 MHz, which is a measure of the amount a photon's frequency can deviate from the transition frequency and still be absorbed by the atom. Therefore, to ensure reliable coupling between the atomic levels, the laser linewidth must be less than the atomic linewidth. Similarly, the cavity length must be stablized to ensure that the resonant cavity frequency is at fixed detuning from the transition frequency.

In our lab, there are currently seven lasers that need to be locked: The MOT laser, the optical lattice laser, the probe laser, the cavity-probe laser, the transfer cavity laser, the repumper laser, and the reference laser. There are two cavities that need to be locked: the experimenal cavity and the transfer cavity. The reference laser is termed the reference laser because it is used as a reference when locking other lasers. To lock a laser to the reference laser, we observe the beatnote signal between the laser and the reference laser and lock using a frequency off-set lock. There are two types of frequency off-set locks in our lab: delay line locks (DLLs) and phase loop locks (PLLs). We will only discuss the DLL in detail below. The reference laser itself is locked using a Doppler-free dichroic atomic vapor laser lock (DAVLL) scheme [6, 7].

We like like to lock our experimental cavity to the cavity-probe laser, but this would require the cavity-probe laser to be on during the entire duration of the experiment. The near-resonant light would then excite the atoms, which is clearly undesirable. The solution was to build another cavity, the transfer cavity, and lock the experimental cavity to the near-resonant laser via the transfer cavity. As Jon Simon so succinctly stated, the experimental cavity is locked to the transfer laser, which is locked to the transfer cavity, which is locked to the cavity-probe laser which, is locked to the reference laser. The transfer laser is far detuned at 817nm, so there is no concern over unwanted excitations. To lock cavities to lasers or lasers to cavities, we use the Pound-Drever-Hall lock (PDHL) [8].

The basic idea behind locking cavities or lasers is the same: feedback. The process

begins with the generation of an error signal, which feeds back on the laser or cavity. The error signal is set to zero when the laser or cavity is at the desired frequency. Otherwise, based on the error signal, a current controller will adjust the current input to the laser or the piezoelectric driver will change the voltage on the piezo to change the length of the cavity. In this way, the laser frequency or cavity length is constantly adjusted against fluctuations.

4.4.1 Locking the Reference Laser

In DAVLL, we send two counterpropagating beams into a vapor cell of atoms. One beam is a strong pump beam while the other is a weak probe beam. The frequencies of both beams are scanned together. If we measure the absorption of the probe beam on a photodiode, we will find a wide absorption dip with a comparitively sharp peak in the center of the dip. The wide dip occurs because moving atoms absorb light off the resonant frequency ω_0 due to the Doppler shift. For example, an atom moving with velocity $\mathbf{v}$ toward the probe beam will absorb light with frequency $\omega_0 - \mathbf{k} \cdot \mathbf{v}$, where $\mathbf{k}$ is the beam's wavevector. Stationary atoms, however, only absorb light at the resonant frequency. Since the transition in stationary atoms are saturated by the strong pump beam, they cannot absorb light from the probe beam. The moving atoms, however, are not saturated due to the Doppler shift. Hence, the sharp peak is centered at the resonant frequency and has width ≈ 5 MHz, which corresponds to the natural linewidth.

In our system, scanning the laser frequencies will result in six peaks in the wide absorption dip. Three peaks occur due to the excitation of stationary atoms from $F = 3$ to $F = 2', F = 3'$, and $F = 4'$. The other three peaks result from moving atoms due to the Doppler shift and occur equidistant between neighboring stationary peaks. Consider an atom moving toward the pump beam. The atom sees the pump beam's frequency increased by kv and the probe beam's frequency decreased by kv. Let the difference between two resonant frequencies be $\Delta\omega$.If the beam frequency is halfway between two resonant frequencies, then the atoms with velocity $v = \frac{\Delta\omega}{/} 2k$ see a pump beam in resonance with the higher energy level and a probe beam in

resonance with the lower energy level. The pump beam will saturate the transition at the higher energy level so absorption by the probe beam is suppressed. The same thing happens with atoms moving away from the pump beam: the pump beam saturates the transition at the lower energy level. Since this occurs for each pair of neighboring excited states, there are three "crossover" peaks in the spectrum.

We would like to lock the reference laser to the resonant frequencies. That is, we would like to use the absorption spectrum as an error signal so we correct the laser frequency whenever it deviates from the resonance peak. In order to do this, we need our error signals to cross the zero voltage line at the desired frequency, which clearly is not the case with the resonance peaks. To resolve this issue, we apply a constant magnetic field to the sample to split the previously degenerate magnetic sublevels. When the magnetic sublevels are no longer degenerate, the absorption spectrum will be shifted symmetrically about the resonance frequency for σ^+ and σ^- light. Although the light we send in is linearly polarized, we send it through a quarter-wave plate and a polarizing beam splitter (PBS) after it has passed through the atomic cloud. This separates the linearly polarized light into its σ^+ and σ^- components. We collect each polarization at a photodiode and subtract one signal from the other. This places the resonance frequency in the absence of a magnetic field at zero voltage. Since it gives a differential signal, the DAVLL scheme also has the benefit of being insensitive to laser power and atomic density fluctuations. Figure 4-5 shows a typical DAVLL signal. .

4.4.2 Pound-Drever-Hall Lock

The general idea of PDHL is to use a phase shift to generate an error signal and then use feedback to correct either laser frequency or cavity length fluctuations. Our discussion of the PDHL refers to locking a cavity to a laser, but the method is the same for locking a laser to a cavity. In the latter case, the feedback signal goes into the laser rather than the cavity. A standard PDHL setup is shown in figure 4-6. Proper feedback requires knowing which way to adjust the laser frequency when it is off resonance. For example, the reflected intensity of the beam is symmetric about the resonance. Consequently, we can't use the intensity as an error signal, since the

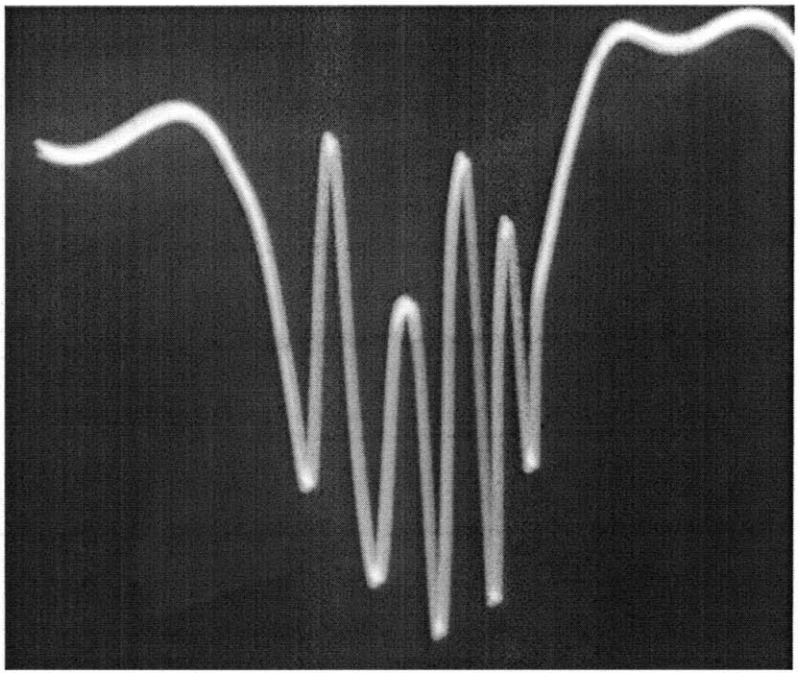

Figure 4-5: DAVLL signal. Here there are only five peaks because the sixth peak is not resolved.

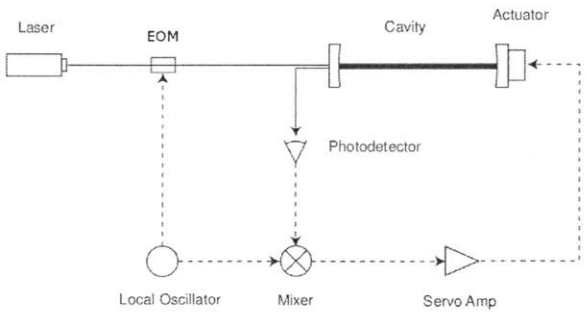

Figure 4-6: Basic PDHL configuration. In our experiment, the actuator is a piezo, driven by the piezoelectric driver, which changes its voltage output to the piezo based on the error signal.

system could not know which way to ajust the frequency when it is off resonance. In other words, our error signal must be an odd function. The PDHL lock creates an odd error signal by phase modulating the beam, giving it sidebands using an electro-optical modulator (EOM). The magnitude of the electric field of our incident beam with the carrier frequency and two sideband frequencies can be written as [9]

$$E_i \approx E_0[J_0(\beta)e^{i\omega_0 t} + J_1(\beta)e^{i(\omega_0+\alpha)t} + J_1(\beta)e^{i(\omega_0-\alpha)t}] \tag{4.10}$$

where β is called the modulation depth, $J_{1,2}(\beta)$ are Bessel fuctions, E_0 is the unmodulated electric field magnitude, ω_0 is the unmodulated field frequency, and the sideband frequencies occur at $\omega \pm \alpha$. The reflection coefficient of a lossless symmetric cavity of length L is

$$F(\omega) = \frac{r(e^{\frac{i\omega L}{c}} - 1)}{1 - r^2 e^{\frac{i\omega L}{c}}} \tag{4.11}$$

To find the reflected field, we multiply each component of the incident field by the reflection coefficient at the appropriate frequency

$$\begin{aligned} E_r \approx E_0[F(\omega_0)J_0(\beta)e^{i\omega_0 t} &+ F(\omega_0+\alpha)J_1(\beta)e^{i(\omega_0+\alpha)t} \\ &+ F(\omega_0-\alpha)J_1(\beta)e^{i(\omega_0-\alpha)t}] \end{aligned} \tag{4.12}$$

This reflected field is sent into a photodetector, which detects its intensity, $|E_r|^2$. The intensity of the reflected field contains terms of frequency ω, $\omega + \alpha$ and $\omega - \alpha$. Interference between ω and $\omega + \alpha$ and between ω and $\omega - \alpha$ creates a beatnote with frequency α. We take this signal, mix it with a term $\propto \cos\alpha$, and low pass filter it. The resulting signal is our error signal.

4.4.3 Delay Line Lock

A diagram of the DLL path is in figure 4-7. In the DLL, the beatnote between the laser we wish to lock and the reference laser is input into a photodiode. The ensuing signal is $\propto \cos((\omega_l - \omega_r)t)$, where ω_l is the frequency of the laser we wish to lock and

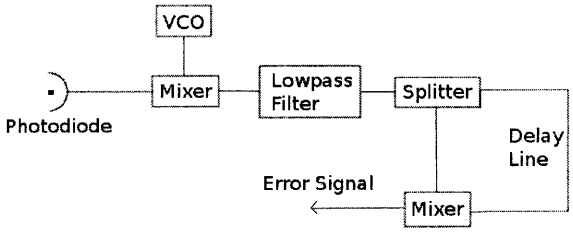

Figure 4-7: Delay line lock configuration. Figure modified from [9].

ω_r is the frequency of the reference laser. [2] Let $\omega_l - \omega_r \equiv \omega$. A voltage controlled oscillator (VCO) produces a signal $\propto \cos((\omega_{VCO}t))$. A mixer is used to multiply the VCO signal and the beatnote signal, giving a signal proportional to

$$\frac{1}{2}[\cos((\omega + \omega_{VC0})t) + \cos((\omega - \omega_{VCO})t)] \tag{4.13}$$

We use a lowpass filter to filter out the $\cos((\omega + \omega_{VC0})t)$ component. A splitter is next used to send the signal through two paths. One path goes straight into a second mixer, and the other path goes through a cable of length L (this is the delay line that this locking scheme derives its name from). Relative the to signal that went directly to the mixer, the signal that goes through the path of length L gains phase so that it is now $\propto \cos((\omega - \omega_{VCO})t + \frac{L}{v}(\omega - \omega_{VCO}))$, where v is the speed of the signal. As before, the mixer multiplies the two signals giving a signal

$$\propto \frac{1}{2}[\cos(2(\omega - \omega_{VCO})t + \frac{L}{v}(\omega - \omega_0)) + \cos(\frac{L}{v}(\omega - \omega_0))] \tag{4.14}$$

Passing this signal through another lowpass filter gives the final signal as

$$\propto \cos(\frac{L}{v}(\omega - \omega_{VCO})) \tag{4.15}$$

By tuning ω_{VCO}, we can shift the signal along the frequency axis so that our desired laser frequency matches where the signal crosses the x-axis. Hence, we can lock a laser to this error signal.

[2] There is also a $\cos((\omega_l + \omega_r)t)$ component, but it oscillates too fast for our photodiode to detect.

Chapter 5

Conclusion

We have discussed the theoretical underpinnings of CIT and the technical aspects of our experiment. We have presented preliminary data on the beam size at our atomic ensemble. We find that the beam size is around $5\mu m$, which is most likely smaller than the atomic cloud size. Since we would like the beam size to be smaller than the atomic cloud size so that the beam maximally interacts with the atoms, we can work with this beam size and move on in the experiment. The next step would be to measure the absorption of the beam on the $F = 4$ to $F = 5'$ transition. This will allow us to obtain the optical depth of our sample. If the sample is not optically dense enough, we will be unable to see even the broad absorption peak of the $F = 3$ to $F = 4'$ transition. Thus far, CIT seems experimentally promising, and we hope to obtain results within a few weeks.

Appendix A

Delay Line Lock Circuit

Our current DLL setup consists of parts from Mini-Circuits. Since this setup is rather space-consuming, we attempted to put all the DLL components on a circuit board. The PCB layout and schematic are shown below. However, there were oscillation problems with the circuit, which may have been caused by excessive gain in the circuit. The table below shows the DLL input frequencies and the frequencies at which signal oscillations occur as the VCO is tuned.

Input Frequency (MHz)	Frequency Range where oscillations occur (MHz)	(see prev column)	(see prev column)
700	1342-1410	–	–
750	1070-1132	1228-1242	1453-1484
800	1172-1209	1307-1329	1540-1614
850	1342-1410	1117-1280	1640-1720
900	1182-1212	1740-1810	–
950	1244-1270	1815-1907	–
1000	1934-2009	–	–

Table A.1: Oscillations

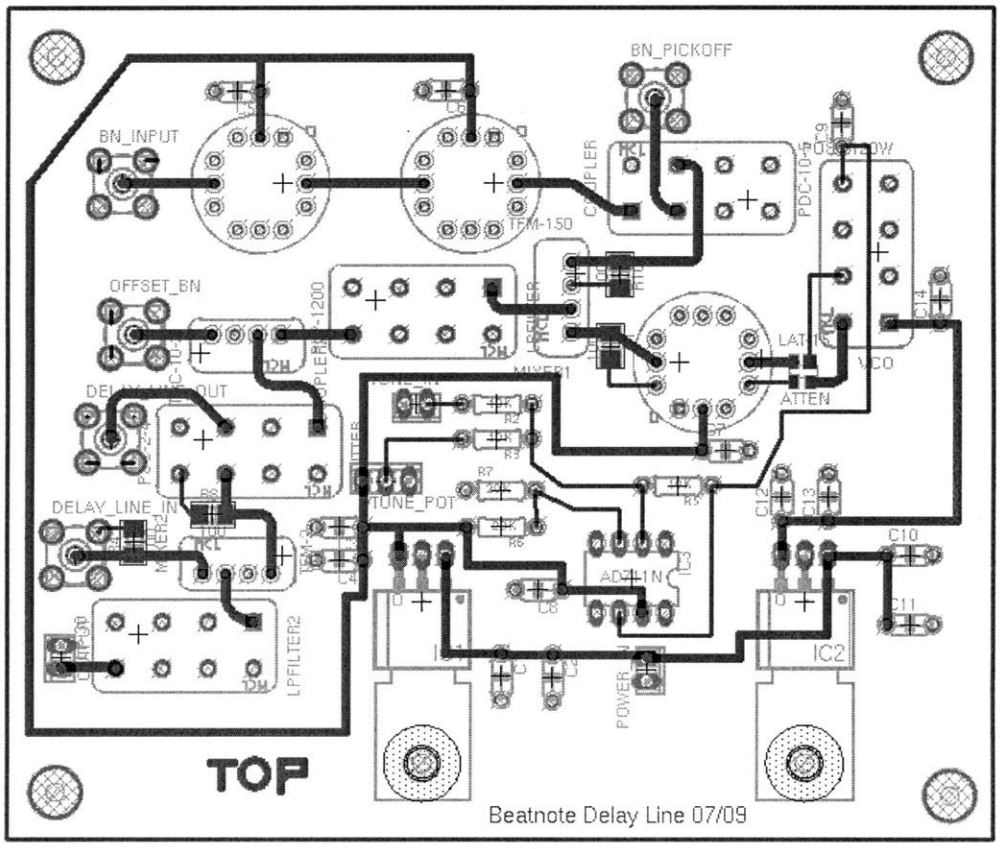

Figure A-1: PCB layout of the DLL circuit

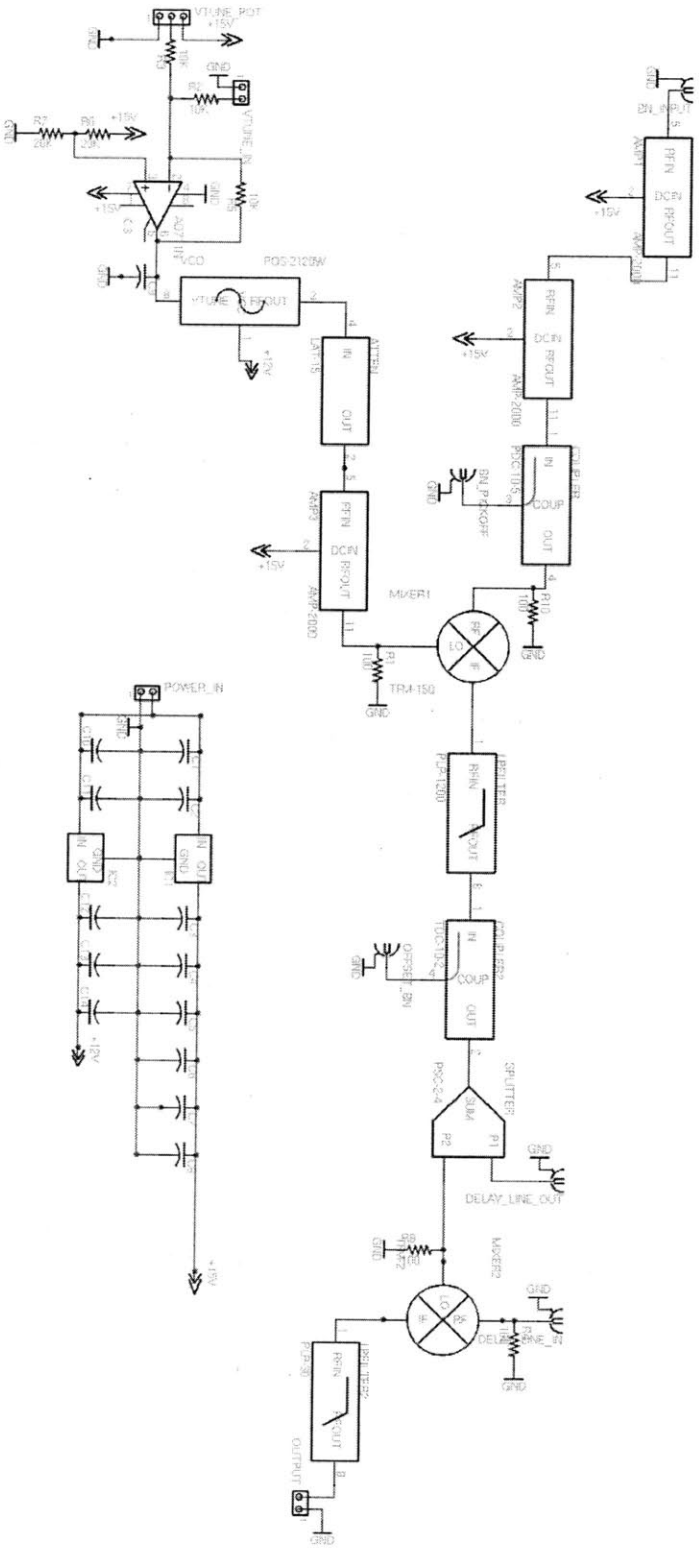

Figure A-2: Schematic of the DLL circuit

Appendix B

920 vs. 937 Optical Lattice Laser

We currently use a 937nm Eagleyard laser for our optical lattice. However, these lasers have a had a habit of spontaneous deaths and unstable lasing [14]. Hence, we have built a 920nm laser as back-up. In order to measure the finesse of the cavity at 920nm, we need to know the cavity linewidth. Usually, the cavity linewidth is measured by monitoring the cavity transmission as we sweep through the cavity linewidth with a laser frequency modulated with sidebands. However, since our cavity linewidth is much narrower than our laser linewidth, this technique cannot be used. Instead, we measured the linewidth of the cavity at 920nm using the ringdown method described by Poirson et al. [15]. In this method, we monitor the cavity transmission as we rapidly sweep the cavity resonance through the laser line via the piezo. We obtain plots like that of figure B-1.

The data gives us the cavity linewidth through the following equation:

$$\frac{\kappa}{\pi} = \frac{1}{2\pi}\frac{R+2-e}{2\Delta t} \tag{B.1}$$

where R is ratio between the heights of two peaks time Δt apart. Table B.1 gives a summary of results for five sets of data.

The finesse of the cavity is given by

$$F = \frac{FSR}{\text{cavity linewidth}} \tag{B.2}$$

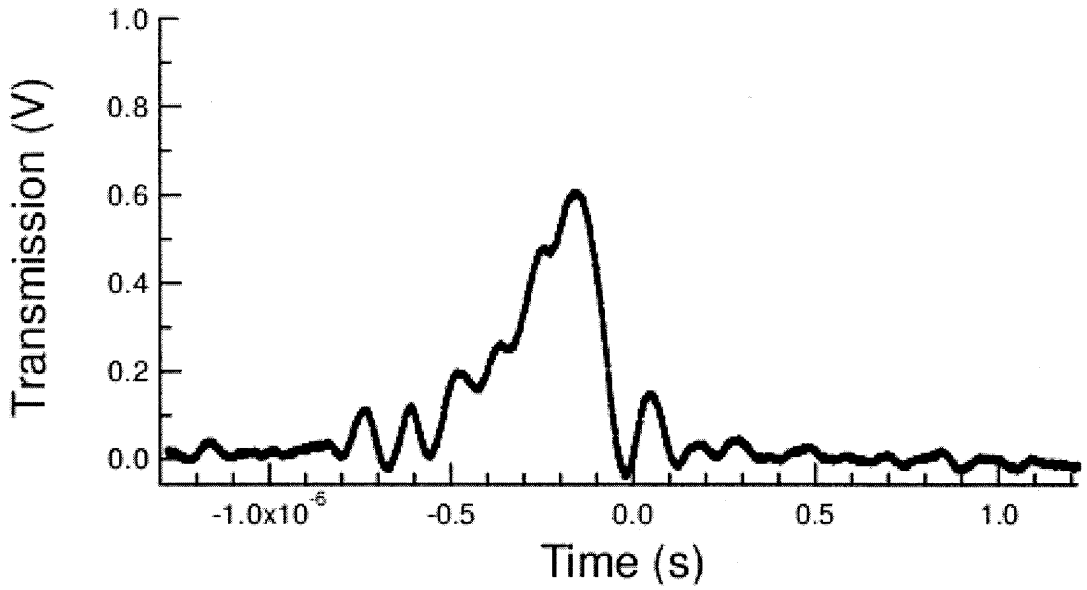

Figure B-1: Data obtained through ringdown method. Cavity piezo was scanned with 20 kHz, 10 Vpp signal

	Height 1	Height 2	$\triangle t$ (ms)	Cavity Linewidth (MHz)
Data Set 1	0.5	0.06	210	2.9
Data Set 2	0.6	0.144	197	1.4
Data Set 3	0.54	0.12	180	1.7
Data Set 4	424	51	190	3.1
Data Set 5	532	88	210	2.0

Table B.1: Ringdown data for cavity linewidth measurements. Data Sets 4 and 5 taken at 30 kHz, Data sets 1 through 3 taken at 20 kHz

where FSR is the free-spectral range of the cavity, which is 10.909 GHz for our cavity.

We find a finesse of around 3000, about 10 times better than the finesse at 937nm.

Appendix C

920nm Laser Mount

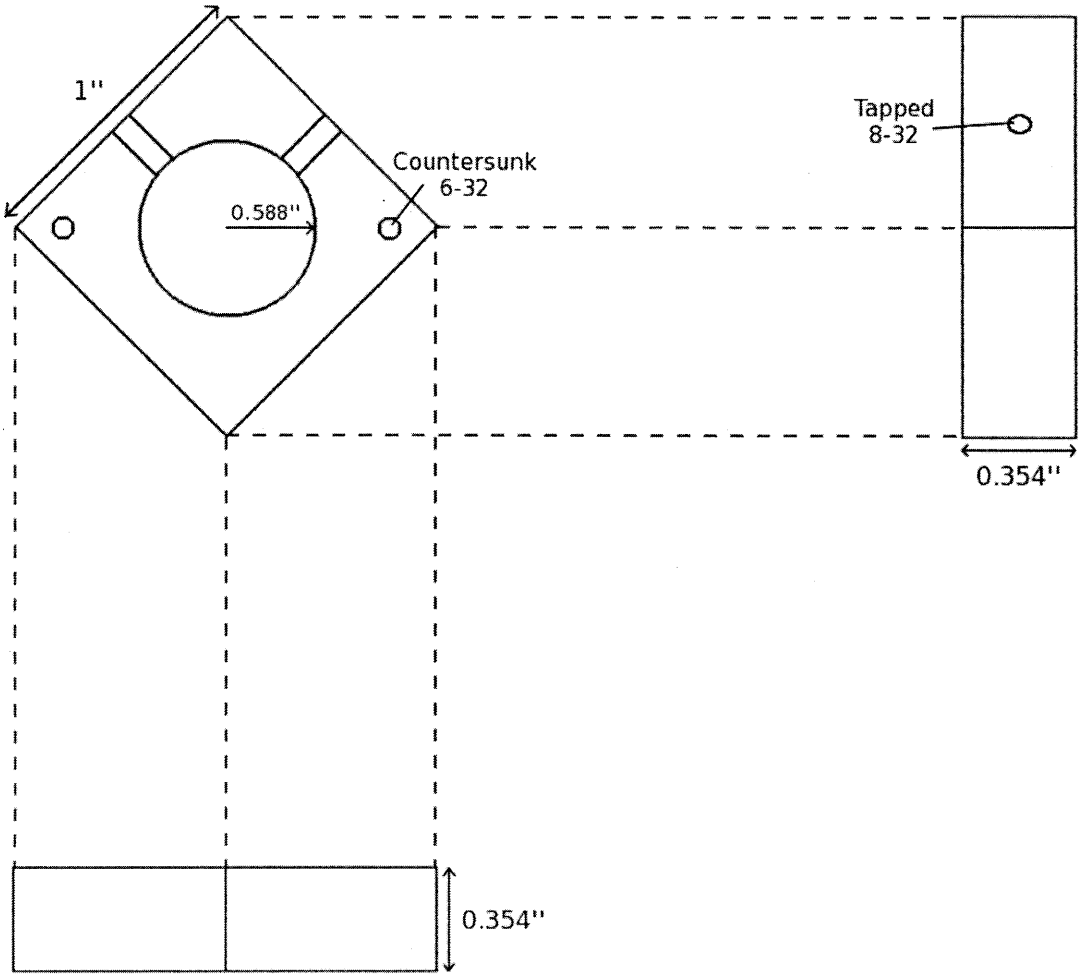

Figure C-1: Machined aluminum mount for the 920nm laser.

Bibliography

[1] Daniel A. Steck *Quantum and Atomic Optics*, available online at http://steck.us/teaching (2006)

[2] M. Scully and M. Zubairy. *Quantum Optics* Cambridge University Press, 2007.

[3] H. Metcalf and P. van der Straten *Laser Cooling and Trapping* Springer-Verlag New York, 1999.

[4] Lecture notes. Physics 285b. Harvard University, Fall 2010

[5] J. Dalibard and C. Cohen-Tannoudji. Laser cooling below the Doppler limit by polarization gradients: simple theoretical models. *Journal of the Optical Society of America*, 6(11): 20232045, 1989.

[6] T. W. Hansch, I. S. Shahin, and A. L. Schawlow. High-resolution saturation spectroscopy of the sodium d lines with a pulsed tunable dye laser. *Phys. Rev. Lett.*, 27(11): 707710, Sep 1971.

[7] A. Hecker, M. Havenith, C. Braxmaier, U. Strner, and A. Peters. High resolution doppler-free spectroscopy of molecular iodine using a continuous wave optical parametric oscillator. *Optics Communications*, 218(1-3):131 134, 2003.

[8] R.W.P Drever *et al.*, Laser phase and frequency stabilization using an optical resonator. *Appl. Phys. B: Photophy. Laser Chem.* 31: 97-105, 1983.

[9] E. Black. An introduction to Pound-Drever-Hall laser frequency stabilization. *Am. J. Phys.*, 69(1): 79-87, Jan 2001

[10] B. Bloom. Atomic quantum memory for photon polarization. Bachelors thesis, Massachusetts Institute of Technology, 2008.

[11] Daniel A. Steck. Cesium d line data. Technical report, Los Alamos National Laboratory, 1998.

[12] D.Budker et al., Resonant nonlinear magneto-optical effects in atoms. *Reviews of Modern Physics.* 74(4), (2002)

[13] S. E. Harris. *Physics Today.* 50(7): 36-42, 1997.

[14] J. Simon. Cavity QED with Atomic Ensembles. PhD Thesis, Harvard University, 2010.

[15] Jerome Poirson, Fabien Bretenaker, Marc Vallet, and Albert Le Floch. Analytical and experimental study of ringing effects in a fabryperot cavity. application to the measurement of high finesses. *J. Opt. Soc. Am. B*, 14(11): 28112817, 1997.

[16] R. Grimm and M. Weidemuller. Optical dipole traps for neutral atoms. *Adv. At. Mol. Opt. Phys.*. 42: 95-170, February 2000

[17] Dressed-atom approach to atomic motion in laser light: the dipole force revisited. *J. Opt. Soc. Am. B*, 2(11): 1707-1720, Nov 1985